RF Pulse Design: SLR Algorithm, Spectral-Spatial Pulses, 2D and 3D Pulses

John M. Pauly
Magnetic Resonance Systems Research Laboratory,
Stanford University

1 Introduction

RF pulses are the most flexible components of MR pulse sequences. Magnetization can be selectively produced, refocused, and manipulated as a function of space and frequency, as well as MR parameters such as T_1 and T_2. The design of RF pulses is in general a difficult non-linear problem. However, for most cases of interest there are simple, easily computable solutions.

A linear analysis directly analogous to the k-space description of imaging is sufficient for the design of small-tip angle excitation pulses in one and multiple dimensions. Large-tip angle pulses can also be designed with linear methods if certain symmetry requirements are met. The design of 1D large tip angle pulses is a non-linear problem, which can be directly solved with the Shinnar-Le Roux (SLR) algorithm. Non-linear multidimensional pulses can be designed by using the SLR algorithm in one dimension, and linear designs in the remaining dimensions. This includes the important special case of spectral-spatial spin-echo pulses.

There are several different useful approximations for RF pulse design. The small-excitation approximation assumes that M_z is not significantly changed. This produces the familiar transform relationship between a slice profile and an RF pulse.

Such methods based on calculating a magnetization are limited, however, since this is insufficient to fully characterize the rotation produced by an RF pulse. A more convenient approach uses the spinor representation of rotations, which only requires two complex numbers to completely characterize the rotation. Given the spinor, the effect of the RF pulse on any initial magnetization can be calculated. In addition, a small-rotation solution may be obtained, with the small-excitation solution as a special case. Since it can be applied to any initial magnetization, this solution allows large-tip-angle RF pulses to be constructed by concatenating small rotation solutions. This is particularly useful for multidimensional pulses.

Another very important tool is the "hard pulse approximation," which models an RF pulse as a sequence of impulses separated by free precession intervals. This is the basis of the Shinnar-Le Roux algorithm, which allows the exact solution for most 1D RF pulses used in practice.

2 Small-Excitation Approximation

The Bloch equation in the absence of relaxation is written,

$$\frac{d\mathbf{M}}{dt} = \gamma \begin{pmatrix} 0 & \mathbf{G}(t)\cdot\mathbf{x} & -B_{1,y}(t) \\ -\mathbf{G}(t)\cdot\mathbf{x} & 0 & B_{1,x}(t) \\ B_{1,y}(t) & -B_{1,x}(t) & 0 \end{pmatrix} \mathbf{M} \tag{1}$$

where $B_1(t) = B_{1,x}(t) + iB_{1,y}(t)$ and $\mathbf{G}(t) = (G_x(t), G_y(t), G_z(t))^T$. For the case of an initially fully relaxed magnetization aligned with the $+z$ axis, $\mathbf{M}(0) = (0, 0, M_0)^T$. If the RF flip angle is small, the transverse magnetization M_{xy} after an RF pulse of duration T is given by

$$M_{xy}(\mathbf{x}, T) = iM_0 \int_0^T \gamma B_1(t) e^{i\mathbf{k}(t)\cdot\mathbf{x}} dt \tag{2}$$

where $\mathbf{k}(t)$ is a spatial frequency variable given by the integral of the remaining gradient area

$$\mathbf{k}(t) = -\gamma \int_t^T \mathbf{G}(s) ds. \tag{3}$$

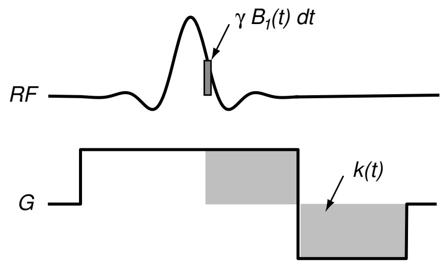

Figure 1: Small-excitation approximation. Each incremental segment of the RF, $\gamma B_1(t)dt$, produces transverse magnetization independently. These then precess under the influence of the remaining gradient. The integrated remaining gradient is $\mathbf{k}(t)$, so the accumulated phase shift is $e^{i\mathbf{k}(t)\cdot\mathbf{x}}$. The slice profile expression in Eq. 2 integrates over all of the incremental segments.

Hence, the transverse magnetization is the transform of the applied RF energy along a k-space trajectory determined by the gradient waveform [1].

2.1 Slice-Selective Excitation

This has a simple interpretation in one dimension, which is illustrated in Fig. 1. If we assume that the RF waveform is partitioned into small segments that each act independently, each segment produces a small amount of transverse magnetization. This magnetization precesses under the effect of the applied gradient, and accrues a phase proportional to the integral of the remaining gradient. The total magnetization is the integral of the contributions of all of these small segments of RF.

For the case of a constant gradient, the slice profile is the transform of the RF waveform. An example is shown in Fig. 2, where the RF waveform (left) has been chosen such that its frequency spectrum excites a well defined slice (right). This is a Hamming windowed sinc waveform, commonly used as an excitation pulse. The excitation angle here is 30°.

A useful concept for selective excitation is the "time-bandwidth product," TBW, which is duration of the pulse multiplied by width of the passband. Pulses with the same time-bandwidth product have the same shape, even if they have different durations. The example in Fig. 2 has a time-bandwidth product of 8. Typically this is the number of zero crossings of the RF waveform, which is also 8 for this example. With a $TBW = 8$, a 4 ms pulse has a bandwidth of $8/4 = 2$ kHz. With a 1

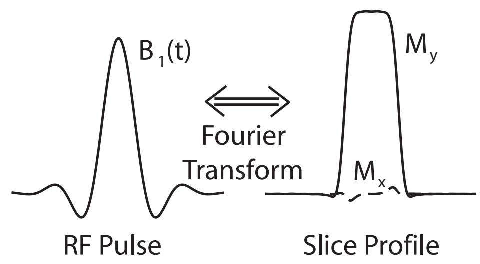

Figure 2: A small-excitation RF pulse (left) and slice profile (right).

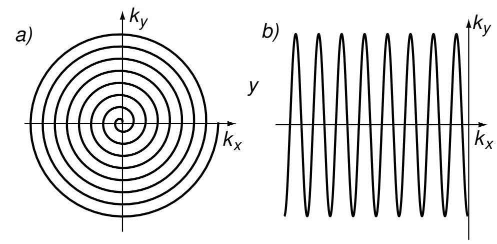

Figure 3: A spiral k-space trajectory (a) and an EPI trajectory (b). As a direct parallel to the imaging case, either of these can be used as the basis of a 2D RF pulse. Many other trajectories are also possible.

G/cm gradient, or 4.257 kHz/cm, this is a little less than a 5 mm slice.

2.2 Multidimensional Selective Excitation

For non-constant gradients and in multiple dimensions the k-space velocity should be normalized

$$M_{xy}(\mathbf{x},T) = iM_0 \int_0^T \frac{\gamma B_1(t)}{|\gamma \mathbf{G}(t)|} e^{i\mathbf{k}(t)\cdot\mathbf{x}} |\gamma \mathbf{G}(t)| dt. \quad (4)$$

The $\mathbf{G}(t)$ is chosen to trace out a pattern that uniformly covers a region of k-space [1]. Two common examples are shown in Fig. 3. As in imaging, the rate at which this pattern is traced out varies due to the limitations of the gradient system hardware. As a result, the RF waveform that should be applied is the sampled transform of the desired profile, compensated by the k-space velocity. An additional compensation term is required if the k-space trajectory is non-uniform [2,3], just as in imaging.

The excited volume can be shifted to any position $\mathbf{x_0}$ by modulating the RF waveform with $e^{-i\mathbf{k}(t)\cdot\mathbf{x}_0}$. Effectively, this keeps the point $\mathbf{x}_0$ exactly on resonance as the gradient waveform is played out.

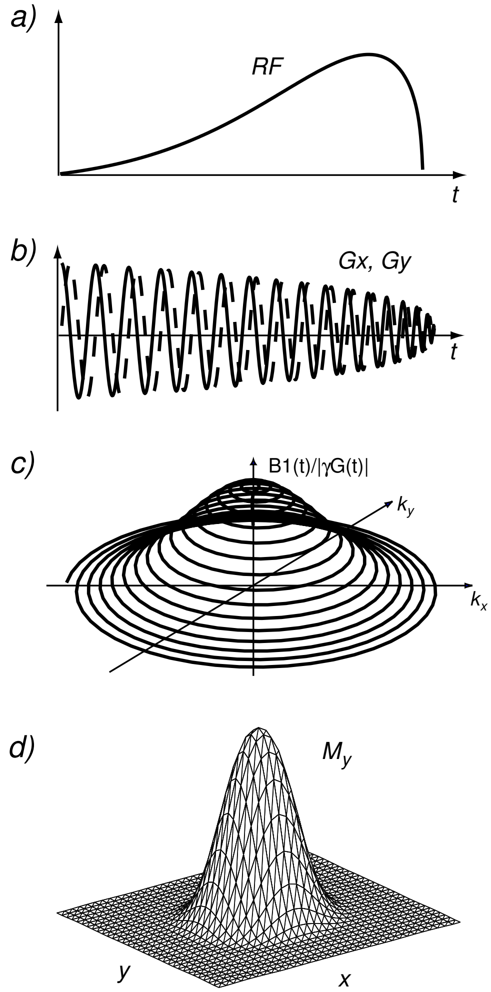

Figure 4: 2D RF pulse (a), gradients (b), k-space weighting (c), and excitation profile (d).

An example multidimensional RF pulse is shown in Fig. 4. This is a 2D selective excitation pulse based on a spiral gradient. The gradient spirals in to the center so that no refocusing lobe is required. This pulse excites a cylinder, limited in $x - y$ plane, and extending in z.

This type of pulse is often used to restrict excitation to a single column or "pencil" to allow tracking of very rapid motion, such as in MR m-mode [4–7] or MR Doppler [8–10]. It is also frequently used for navigator acquisitions [11, 12].

3 Spinors

The Bloch equation in the absence of relaxation reduces to a sequence of rotations. Although we can solve for these rotations by multiplying 3x3 matrices, there is a much simpler representation using 2x2 complex matrices and spinors [13]. A rotation by an angle ϕ about an axis $\mathbf{n} = (n_x, n_y, n_z)^T$ is represented by the matrix

$$Q = \begin{pmatrix} \alpha & -\beta^* \\ \beta & \alpha^* \end{pmatrix} \tag{5}$$

where

$$\alpha = \cos(\phi/2) - i\, n_z \sin(\phi/2) \tag{6}$$
$$\beta = -i\,(n_x + i\, n_y) \sin(\phi/2). \tag{7}$$

These satisfy the constraint

$$\alpha\alpha^* + \beta\beta^* = 1. \tag{8}$$

Note that the rotation angle appears as a half-angle in Eq. 7. The effect of a sequence of rotations is computed by multiplying out the 2x2 complex matrices. Note that the matrix is completely determined by the first column $(\alpha, \beta)^T$, so that a pair of complex numbers is all that is needed to represent a rotation.

Once the rotation produced by an RF pulse has been computed, we would like to know what effect it has given some initial magnetization. Although the derivation of these relationships is complex, the results are very simple. For an excitation pulse, given an initial magnetization of $\mathbf{M} = (0, 0, M_0)^T$, we would like to know the transverse magnetization. This is given by

$$M_{xy}^+ = 2\alpha^*\beta M_0. \tag{9}$$

For an inversion or saturation pulse, the initial magnetization is the same, but we are concerned with the longitudinal magnetization. This is given by

$$M_z^+ = (1 - 2\beta\beta^*)M_0. \tag{10}$$

Spin-echo pulses produce two terms, the spin echo and the unrefocused magnetization which is usually suppressed with dephasing gradients. If we assume the initial magnetization is along $+y$, the spin-echo component is

$$M_{xy}^+ = i\,\beta^2 M_0. \tag{11}$$

Given α, β, and the initial magnetization, it is very easy to compute the final magnetization for most types of RF pulses.

4 Small-Rotation Approximation

A 2x2 spinor version of Eq. 1 can also be written, and solved for the small rotation case, analogous to Eq. 4 [14]. The differential equation is

$$\frac{d}{dt}\begin{pmatrix}\alpha\\ \beta\end{pmatrix} = \frac{i\gamma}{2}\begin{pmatrix}\mathbf{G}(t)\cdot\mathbf{x} & B_1^*(t)\\ B_1(t) & -\mathbf{G}(t)\cdot\mathbf{x}\end{pmatrix}\begin{pmatrix}\alpha\\ \beta\end{pmatrix}. \tag{12}$$

If we assume that that the total rotation is small we can obtain the small-angle approximation

$$\alpha(\mathbf{x},T) = e^{-\frac{i}{2}\mathbf{k}(0)\cdot\mathbf{x}} \tag{13}$$

$$\beta(\mathbf{x},T) = \frac{i}{2}e^{-\frac{i}{2}\mathbf{k}(0)\cdot\mathbf{x}}\int_0^T \gamma B_1(t)e^{i\mathbf{k}(t)\cdot\mathbf{x}}dt \tag{14}$$

where $\mathbf{k}(t)$ is defined as above in Eq. 3. Combining these two expressions with Eq. 9 produces Eq. 2.

If the k-space trajectory starts and ends at the origin, $\mathbf{k}(0) = \mathbf{k}(T) = 0$, and

$$\alpha(\mathbf{x},T) = 1 \tag{15}$$

$$\beta(\mathbf{x},T) = \frac{i}{2}\int_0^T \gamma B_1(t)e^{i\mathbf{k}(t)\cdot\mathbf{x}}dt. \tag{16}$$

If the k-space trajectory is symmetric and the applied RF weighting is hermitian symmetric, then the integral is real. The magnetization at every spatial position is rotated about the same axis, but by different rotation angles. From Eq. 7

$$\phi(\mathbf{x},T) = 2\sin^{-1}(\beta(\mathbf{x},T)). \tag{17}$$

This is important because it allows us to design large-flip angle multidimensional pulses as a sequence of small rotations. In fact, the spiral 2D pulse of Fig. 4 continues to work well at flip angles of π [14]. This does not hold for pulses based on echo-planar trajectories. However, the small-rotation approximation is a useful building block for the solution of large-tip-angle echo-planar pulses, as will be described below.

5 Hard-Pulse Approximation and the Shinnar-Le Roux Algorithm

The very important hard-pulse approximation [15–21] allows the complete solution of 1D RF pulse design problems for most cases of interest in MRI. The basic idea is that each segment of a sampled RF pulse is assumed to occur instantaneously, followed by a brief interval of free precession. In this case, the rotation produced by the j^{th} sample of the RF pulse is represented by

$$Q_j = \begin{pmatrix} C_j & -S_j^*\\ S_j & C_j\end{pmatrix}\begin{pmatrix} z^{1/2} & 0\\ 0 & z^{-1/2}\end{pmatrix} \tag{18}$$

where

$$C_j = \cos(\gamma|B_{1,j}|\Delta t/2) \tag{19}$$

$$S_j = ie^{i\angle B_{1,j}}\sin(\gamma|B_{1,j}|\Delta t/2) \tag{20}$$

$$z = e^{i\gamma Gx\Delta t}. \tag{21}$$

In order to calculate the cumulative effect of the sequence of rotations, the Q_j are multiplied together. However, only the first column of the rotation matrix needs to be computed. If $(\alpha_{j-1}, \beta_{j-1})^T$ is the spinor after j samples, we can compute

$$\begin{pmatrix}\alpha_j\\ \beta_j\end{pmatrix} = Q_j\begin{pmatrix}\alpha_{j-1}\\ \beta_{j-1}\end{pmatrix}. \tag{22}$$

To eliminate the half powers of z we define

$$A_j = z^{1/2}\alpha_j \tag{23}$$

$$B_j = z^{1/2}\beta_j. \tag{24}$$

We can recursively compute

$$\begin{pmatrix}A_j\\ B_j\end{pmatrix} = \begin{pmatrix} C_j & -S_j^*\\ S_j & C_j\end{pmatrix}\begin{pmatrix} 1 & 0\\ 0 & z^{-1}\end{pmatrix}\begin{pmatrix}A_{j-1}\\ B_{j-1}\end{pmatrix}. \tag{25}$$

This means that an N sample RF pulse can be represented by two polynomials $A_N(z)$ and $B_N(z)$, where $z^{-1} = e^{-i\gamma Gx\Delta t}$. Spatial profiles are computed by evaluating $A_N(z)$ and $B_N(z)$ for $z^{-1} = e^{-i\gamma Gx\Delta t}$ as a function of x, as it varies over the spatial extent of the profile. This is equivalent to computing the Fourier transform of the sequence of coefficients

The significance of this representation is that it is invertible. Given $A_N(z)$ and $B_N(z)$ it is possible to reverse the process and compute the Q_N, and hence the last RF sample, as well as the remaining $A_{N-1}(z)$ and $B_{N-1}(z)$. Applying the procedure recursively produces the entire RF waveform.

This inversion procedure can be used to design RF pulses by designing the $A_N(z)$ and $B_N(z)$. The two polynomials must satisfy the amplitude constraints implicit in Eqs. 7 and 8. From Eq. 7 the function $B_N(z)$ should be chosen to approximate the sine of half the desired rotation angle, with a constant phase determined by the desired rotation axis. The magnitude of $A_N(z)$ is determined by the magnitude constraint Eq. 8. As is shown in [21], a minimum power solution uniquely determines $A_N(z)$ be minimum phase. This is computed by using the Hilbert transform relationship between the log of the magnitude of a minimum phase function and the phase of that function. Once $A_N(z)$ has been computed, the two polynomials are processed using the inversion procedure to produce the RF waveform. This design procedure is the Shinnar-Le Roux algorithm.

An example of this method is shown in Fig. 5, which demonstrates the design of a spin-echo pulse. We start by choosing a $B_N(z)$ that approximates the desired profile. This can be just about any function that could be used as a lowpass digital filter. In this example we use the same Hamming windowed sinc for Fig. 2, which is sometimes itself used as a spin-echo pulse. From Eq. 7 $B_N(z)$ must be scaled so that the passband has an amplitude of $\sin\phi/2 = \sin\pi/2 = 1$. This is plotted in Fig. 5. The $A_N(z)$ polynomial is then computed by the magnitude constraint, Eq. 7, and the minimum power criteria. The RF pulse is then computed using the SLR inversion procedure. The resulting RF pulse and spin-echo profile are also shown in Fig. 5c and d.

Although this procedure may appear complex, it is actually very simple. The slice profile is determined by $B_N(z)$, which is designed as RF pulses themselves have traditionally been designed, using Fourier transform arguments. The flip angle is determined by the scaling of $B_N(z)$. The rest of the procedure is deterministic, and can be considered a black box. For convince, we'll denote this black box as the "inverse SLR transform",

$$B_1(t) = \mathcal{SLR}^{-1}(B_N(z)). \qquad (26)$$

6 One Dimensional Pulses

A wide variety of types of RF pulses can be designed by using different initial $B_N(z)$ polynomials. The main considerations are what the pulse will be used for, and whether the slice profile phase can be exploited.

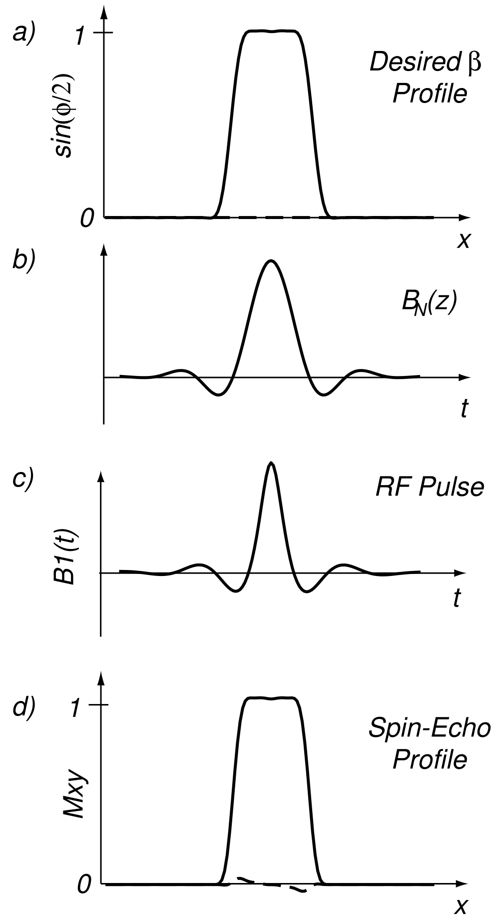

Figure 5: Illustration of the design process in the SLR algorithm. In (a) the profile of $B_N(z)$ is chosen and scaled to produce the right flip angle. The transform of this profile is the $B_N(z)$ polynomial (b). The inverse SLR transform $\mathcal{SLR}^{-1}(B_N(z))$ produces the spin-echo RF pulse (c). The profile of the refocused magnetization is shown in (d).

6.1 Linear-Phase Pulses

Slice-selective excitation pulses and spin-echo pulses have maximum signal if the phase across the slice is linear. A linear-phase excitation pulse is perfectly refocused with a gradient reversal. A linear-phase RF pulse is produced by starting with a linear phase $B_N(z)$. These are hermitian symmetric about the midpoint, as in Fig. 5.

There are two costs for linear phase. One is that a linear-phase pulse also maximizes the peak RF power. Another is that the slice profile is not as selective as minimum/maximum phase or non-linear phase pulses can be.

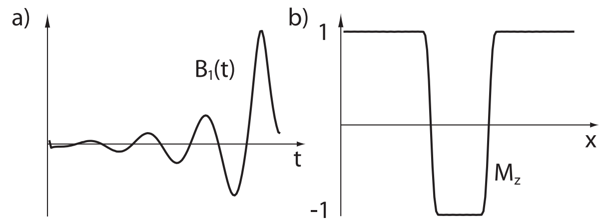

Figure 6: Minimum-phase inversion pulse (left) and inversion profile (right).

6.2 Minimum/Maximum-Phase Pulses

For other types of pulses, the phase of the profile is not an issue. This is true of inversion pulses and saturation pulses, where any transverse magnetization is generally suppressed with a dephasing gradient. In this case, we can improve the selectivity of the profile by starting with a minimum or maximum phase design. This can be almost twice as selective as a linear-phase pulse for the same duration.

A minimum phase pulse has most of the RF energy at the end of the pulse. A maximum-phase pulse is a minimum-phase pulse played in reverse order. An example of a minimum-phase inversion pulse is shown in Fig. 6.

6.3 Nonlinear-Phase Pulses

While minimum and maximum phase pulses have sharper slice profiles than linear-phase pulses, they require very close to the same peak power. Peak power is often the primary practical concern when designing pulses. Lower peak power can often be obtained by using a non-linear phase RF pulse [22, 23]. These can be designed by starting with a minimum phase $B_N(z)$. If this has a time-bandwidth product of M, there are 2^M possible phase profiles that have an identical magnitude profile. These can be searched to optimize a particular parameter, such as peak RF power. An example of an inversion pulse designed with this approach is shown in Fig. 7, along with the minimum phase pulse with the identical profile. In this case the peak amplitude has been reduced to 56%. Note that the integrated power remains the same. The use of nonlinear phase simply distributes this power more uniformly along the length of the pulse.

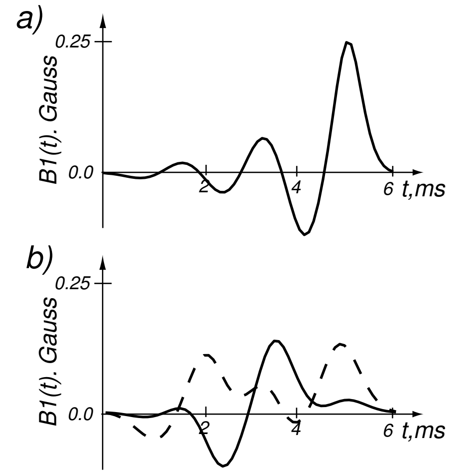

Figure 7: Comparison of a minimum phase and an optimized non-linear phase inversion pulses. Both pulses have identical inversion profiles. The optimized nonlinear phase pulse has 56% of the amplitude of the minimum phase pulse, or 31% of the peak power. The integrated power of the two pulses is identical.

For higher time-bandwidth pulses, exhaustive searches become impractical. A preferred approach is to choose a target quadratic phase profile, and construct $B_N(z)$ so as to closely approximate this profile. This is the approach used by Le Roux in the design of his Very Selective Saturation (VSS) pulses [24, 25].

7 Echo-Planar and Spectral-Spatial Pulses

The second example k-space trajectory in Fig. 3 is EPI. This can be used as the basis of a 2D spatial excitation RF pulse, using exactly the same approach as for the spiral pulse shown in Fig. 4. This has been used as an excitation pulse for 2D saturation [26] and to limit the FOV for fast imaging.

An important extension of echo-planar based designs is the spectral-spatial pulse [27] which is simultaneously selective in both space and frequency. Spectral-spatial pulses are used for lipid suppression for fast EPI or spiral imaging, where lipids would otherwise produce image artifacts [28]. In addition, they can be used in fast spin-echo imaging to eliminate the bright fat effect [29]. Finally, they can be used for water suppression in spectroscopic imaging [30, 31].

A spectral-spatial pulse is based on a conventional echo-planar k-space trajectory. For a 2D spatial pulse the constant gradient in the "phase-encode" direction establishes a linear distribution of frequencies, and the RF pulse selects a range of these frequencies. For a spectral-spatial pulse, we use the same RF pulse, but eliminate the constant gradient. This leaves us with a pulse that is frequency selective to the naturally occuring sources of frequency shifts such as chemical shift and susceptibility shifts.

While spectral-spatial pulses can be designed using the small-excitation approximation, as in Fig. 4, this approach degrades as the flip angle increases. For spin-echo or inversion pulses, the nonlinearity of the Bloch equation must be considered. An effective approach is to use an SLR design in the spectral dimension, and the small-rotation approximation in the spatial domain [32]. Spin-echo pulses designed with this approach can produce excellent water suppression for MRSI experiments [30–32]. Figure 8 is a spin-echo pulse designed with this approach. Another approach is a full 2D SLR design [33]. By replacing the 1D subpulses with 2D spirals, a 3D pulse, or a 2D spatial, 1D spectral pulse can also be produced [34].

Spectral-spatial pulses have some interesting properties. They don't exhibit displacement with frequency offset [29]. The spectral-spatial pulse spatial profile is only perfect exactly on resonance, but this point can be shifted in the design to improve performance at any particular point. This is useful for improving the depth of a stopband [32] or eliminating an N/2 sidelobe [35]. In addition, simplified designs can be based on conventional slice selective pulses with trapezoidal gradients [36]. By using only alternate gradient lobes, the flow performance is also improved.

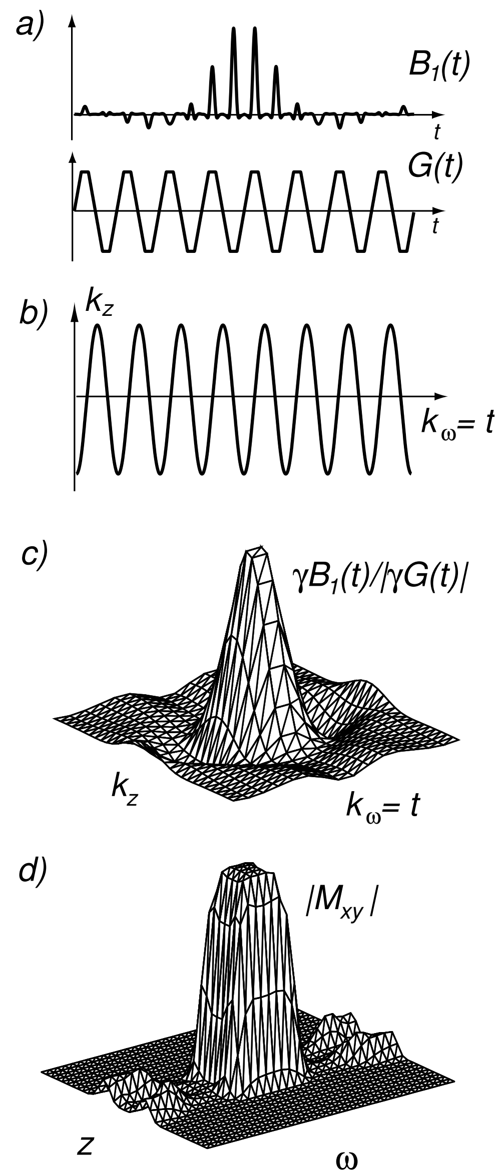

Figure 8: Spectral-Spatial spin-echo RF pulse and gradient, k-space trajectory (b), k-space weighting (c), and spin-echo profile (d).

References

[1] J.M. Pauly, D.G. Nishimura, and A. Macovski. A **k**-space analysis of small tip excitation. *J. Magn. Reson.*, 81:43–56, Jan 1989.

[2] C.J. Hardy, H.E. Cline, and P.A. Bottomley. Correcting for nonuniform *k*-space sampling in two-dimensional NMR selective excitation. *J. Magn. Reson.*, 87:639–645, 1990.

[3] C. J. Hardy and P. A. Bottomley. 31P spectroscopic localization using pinwheel NMR excitation pulses. *Magn Reson Med*, 17(2):315–27, 1991.

[4] H. E. Cline, C. J. Hardy, and J. D. Pearlman. Fast MR cardiac profiling with two-dimensional selective pulses. *Magn Reson Med*, 17(2):390–401, 1991.

[5] J. D. Pearlman, C. J. Hardy, and H. E. Cline. Continual NMR cardiography without gating: M-mode MR imaging. *Radiology*, 175(2):369–73, 1990.

[6] C. J. Hardy, B. D. Bolster, E. R. McVeigh, I. E. Iben, and E. A. Zerhouni. Pencil excitation with

interleaved fourier velocity encoding: NMR measurement of aortic distensibility. *Magn Reson Med*, 35(6):814–9, 1996.

[7] K. Butts, N. J. Hangiandreou, and S. J. Riederer. Phase velocity mapping with a real time line scan technique. *Magn Reson Med*, 29(1):134–8, 1993.

[8] P. Irarrazabal, B. S. Hu, J. M. Pauly, and D. G. Nishimura. Spatially resolved and localized real-time velocity distribution. *Magn Reson Med*, 30(2):207–12, 1993.

[9] B. S. Hu, J. M. Pauly, and D. G. Nishimura. Localized real-time velocity spectra determination. *Magn Reson Med*, 30(3):393–8, 1993.

[10] G. T. Luk Pat, J. M. Pauly, B. S. Hu, and D. G. Nishimura. One-shot spatially resolved velocity imaging. *Magn Reson Med*, 40(4):603–13, 1998.

[11] Y.L. Liu, S.J. Riederer, P.J. Rossman, R.C. Grim, J.P. Debbins, and R.L. Ehman. A monitoring, feedback, and triggering system for reproducible breath-hold MR imaging. *Magn. Reson. Med.*, 30(4):507–11, 1993.

[12] Y. Wang, P.J. Rossman, R.C. Grimm, S.J. Riederer, and R.L. Ehman. Navigator-echo-based real-time respiratory gating and triggering for reduction of respiration effects in three-dimensional coronary MR angiography. *Radiology*, 198(1):55–60, 1996.

[13] E. T. Jaynes. Matrix treatment of nuclear induction. *Phys Rev*, 98(4):1099–1105, May 1955.

[14] J.M. Pauly, D.G. Nishimura, and A. Macovski. A linear class of large-tip-angle selective excitation pulses. *J. Magn. Reson.*, 82:571–587, May 1989.

[15] P. Le Roux. French patent 8610179, 1986.

[16] P. Le Roux. Exact synthesis of radiofrequency waveforms. In *Proc. Seventh SMRM*, page 1049, August 1988.

[17] M. Shinnar, S. Eleff, H. Subramanian, and J.S. Leigh. The synthesis of pulse sequences yielding arbitrary magnetization vectors. *Magn. Reson. Med.*, 12:74–80, Oct 1989.

[18] M. Shinnar, L. Bolinger, and J.S. Leigh. The use of finite impulse response filters in pulse design. *Magn. Reson. Med.*, 12:75–87, Oct 1989.

[19] M. Shinnar, L. Bolinger, and J.S. Leigh. The synthesis of soft pulses with a specified frequency response. *Magn. Reson. Med.*, 12:88–92, Oct 1989.

[20] M. Shinnar and J.S. Leigh. The application of spinors to pulse synthesis and analysis. *Magn. Reson. Med.*, 12:93–98, Oct 1989.

[21] J.M. Pauly, P. Le Roux, D.G. Nishimura, and A. Macovski. Parameter relations for the Shinnar-Le Roux RF pulse design algorithm. *IEEE Trans. on Med. Imag.*, 10(1):53–65, 1991.

[22] M. Shinnar. Reduced power selective excitation radio frequency pulses. *Magn Reson Med*, 32(5):658–60, 1994.

[23] S. Pickup and X. Ding. Pulses with fixed magnitude and variable phase response profiles. *Magn Reson Med*, 33(5):648–55, 1995.

[24] P. Le Roux, R. J. Gilles, G. C. McKinnon, and P. G. Carlier. Optimized outer volume suppression for single-shot fast spin-echo cardiac imaging. *J Magn Reson Imaging*, 8(5):1022–32, 1998.

[25] T. K. Tran, D. B. Vigneron, N. Sailasuta, J. Tropp, P. Le Roux, J. Kurhanewicz, S. Nelson, and R. Hurd. Very selective suppression pulses for clinical MRSI studies of brain and prostate cancer. *Magn Reson Med*, 43(1):23–33, 2000.

[26] M. T. Alley, J. M. Pauly, F. G. Sommer, and N. J. Pelc. Angiographic imaging with 2d rf pulses. *Magn Reson Med*, 37(2):260–7, 1997.

[27] C. H. Meyer, J. M. Pauly, A. Macovski, and D. G. Nishimura. Simultaneous spatial and spectral selective excitation. *Magn Reson Med*, 15(2):287–304, 1990.

[28] C.H. Meyer, B.S. Hu, D.G. Nishimura, and A. Macovski. Fast spiral coronary artery imaging. *Magn. Reson. Med.*, 28(2):202–213, December 1992.

[29] W. Block, J. Pauly, A. Kerr, and D. Nishimura. Consistent fat suppression with compensated spectral-spatial pulses. *Magn Reson Med*, 38(2):198–206, 1997.

[30] D. Spielman, J. Pauly, A. Macovski, and D. Enzmann. Spectroscopic imaging with multidimensional pulses for excitation: Simple. *Magn Reson Med*, 19(1):67–84, 1991.

[31] J. Star-Lack, D. B. Vigneron, J. Pauly, J. Kurhanewicz, and S. J. Nelson. Improved solvent suppression and increased spatial excitation bandwidths for three-dimensional PRESS CSI using phase-compensating spectral/spatial spin-echo pulses. *J Magn Reson Imaging*, 7(4):745–57, 1997.

[32] J. Pauly, D. Spielman, and A. Macovski. Echo-planar spin-echo and inversion pulses. *Magn Reson Med*, 29(6):776–82, 1993.

[33] M. H. Buonocore. A Shinnar-Le Roux algorithm for design of 2D and 3D spatially selective RF pulses. In *Proc. Tenth SMRI, in* J. Magn. Reson. Imaging, number 2P, page 145, Mar./Apr. 1992.

[34] J. M. Pauly, B. S. Hu, S. J. Wang, D. G. Nishimura, and A. Macovski. A three-dimensional spin-echo or inversion pulse. *Magn Reson Med*, 29(1):2–6, 1993.

[35] Y. Zur. Design of improved spectral-spatial pulses for routine clinical use. *Magn Reson Med*, 43(3):410–20, 2000.

[36] F. Schick. Simultaneous highly selective MR water and fat imaging using a simple new type of spectral-spatial excitation. *Magn Reson Med*, 40(2):194–202, 1998.